

Fatigue of double-sided welds and welds with controlled melt through for the stiffener-to-deck weld in orthotropic bridge decks

Johan Maljaars

- Department of Reliable Structures, TNO, the Netherlands
- Faculty of the Built Environment, Eindhoven University of Technology, the Netherlands

Orthotropic bridge decks (OBD-s) are sensitive to fatigue failure. Strict tolerances apply to the geometry of one of the critical connections in OBD-s, the stiffener-to-deck welded connection, to obtain high fatigue resistance. These tolerances appear difficult to meet in practice. Two alternatives have been developed recently for this connection, namely a double-sided welded connection and a single-sided welded connection with controlled and continuous melt-through. Both alternatives have the promise of easier fabrication. This paper evaluates the fatigue resistance of these welded connections based on tests collected from the literature and on fracture mechanics calculations. The paper thereby provides the basis for the incorporation of these details into the new Technical Specification TS 1993-1-901, which will be part of the new generation of Eurocodes.

Keywords: Orthotropic bridge deck, stiffener-to-deck weld, rib-to-deck weld, double-sided welded connection, weld melt-through, weld penetration

1 Introduction

Fatigue failures of welded connections in orthotropic bridge decks (OBD-s) in practice [1, 2, 3] and tests have shown that OBD-s are sensitive to fatigue failure. Designing OBD-s for fatigue is therefore an important task for structural engineers. To assist in this task, the Technical Specification TS 1993-1-901 [4] has been developed. This document will be part of the new generation of Eurocodes, and it provides methods to evaluate the fatigue resistance of OBD-s using $S-N$ curves and structural (where possible, hot-spot) stress ranges. One of the most critical connections in OBD-s is the connection between the closed

stiffener (also referred to as the rib) and the deck plate. Four types of fatigue cracks, in line with the standard EN 1993-1-9 [5] referred to as ‘details’, can develop in this connection between crossbeams, and one type can develop at a crossbeam; see Figure 1.

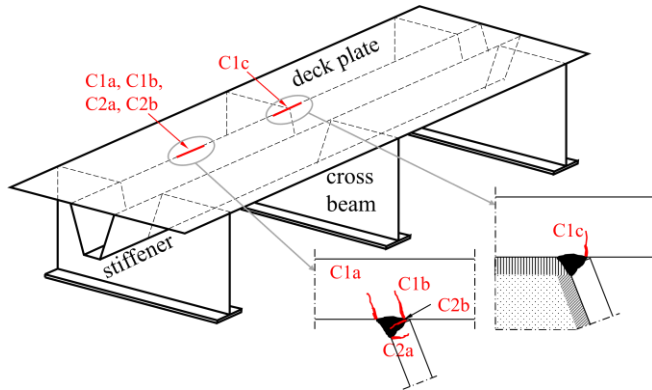


Figure 1. Orthotropic bridge deck with the five fatigue-sensitive details in the traditional, single-sided stiffener-to-deck plate connection

International standards and guidelines such as EN 1993-1-9 [5] and the recommendations from the International Institute of Welding [6] provide characteristic fatigue resistance curves, called ‘ $S-N$ curves’, for weld toes verified using the hot-spot stress method. These characteristic curves are defined with a 95% exceedance probability. However, the 95% exceedance resistance resulting from tests on details in orthotropic bridge decks is often higher than the $S-N$ curves of these standards imply, because of the following reasons [7]:

- The tests on which the $S-N$ curves in standards are based, are loaded in tension–tension with high stress ratios. The details in Figure 1 are loaded in compression or bending, often creating compression at the crack initiation location. Even though residual welding stresses are present, external compression is reported as positively influencing the fatigue resistance [8], especially for larger cracks that have grown out of the zone with high residual tensile stress.
- OBD-s are redundant and tolerable to fatigue cracks, because adjacent elements take over part of the load in case a crack causes loss in flexural rigidity. In Detail C1c (Figure 1), a crack initiates at a location of high stress but, after some growth, it enters an area

with lower stress, giving a reduced crack driving force. This causes the crack growth rates to be relatively low for OBD details.

- The load is multi-directional for some details and the crack mode is not always Mode I [9]. This also causes a relatively low crack growth rate.
- The $S-N$ curves in standards are given for a plate thickness of 25 mm. The stiffeners are substantially thinner, usually between 6 and 8 mm. A beneficial thickness effect may then arise [10].

TS 1993-1-901 [4] therefore gives the hot-spot $S-N$ curves for each detail specifically.

However, the relatively high fatigue resistances are accompanied by strict requirements regarding the geometry of the stiffener-to-deck plate connection. Maljaars et al. [7] provide the background of these strict requirements for the stiffener-to-deck plate connection constructed with a traditional partial penetration weld:

1. The stiffener web should be pressed against the deck plate during welding. Shrinkage of the weld will then ensure firm contact of the tip of the stiffener web and the deck plate, see Figure 2. This contact enables part of the load on the connection to be transferred through the contact point instead of the weld. For practical reasons, the requirement is set to $h_1 = 0$ (see Figure 3 for the definition of h_1) over more than 90% of the weld length. This is requirement important for a high fatigue resistance of Detail C1b. It probably is also important for Detail C2b, but test data lack for confirmation.
2. The weld should be an almost full penetration weld while, on the other hand, it should not result in uncontrolled melt through. The fatigue resistance is based on a selection of tests satisfying $h_2 = 1.0$ mm with a tolerance of -0.5 and $+1.0$ mm (Figure 3). This requirement is majorly important for Detail C2d but it is also important for Detail C1b. In case of a very large lack of penetration, ultimately resulting in a fillet weld, it even has impact on Details C1a, C1c and C2a.
3. The weld should be of sufficient size and the weld flank angles should not be much smaller than 135° . This is established through specifying that $h_3 = t_s \pm 1$ mm and

$h_4 = t_s \pm 1$ mm (Figure 3). Moreover, a smooth transition is required at the weld toes. These requirements are important for Details C1a and C2a.

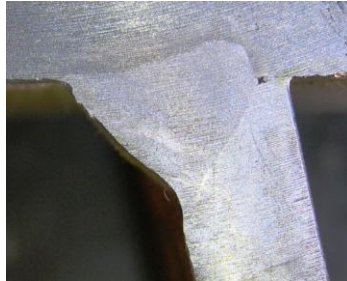


Figure 2. Traditional single-sided partial penetration weld, showing plastic deformation of the tip of the stiffener web. (Figure reproduced from [11])

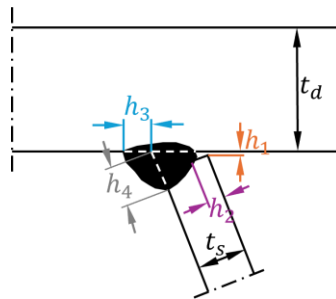


Figure 3. Dimensional parameters of the single-sided partial penetration welded connection

Construction companies have informed that especially Requirements 1 and 2 are difficult to meet. This raises the costs and causes delays and planning uncertainties in constructing OBD-s. On the other hand, these requirements are crucial for ensuring good fatigue performance of OBD-s. Two recent developments in the construction of the stiffener-to-deck connection can overcome the sensitivity of the existing detail to geometric production tolerances. First, a double-sided welded connection was proposed by Japanese researchers [12] and was further developed, tested, and applied in China by Q. Zhang et al. [13, 14, 15]. After constructing the deck with a traditional single-sided partial penetration weld from the outside of the stiffeners, a fully mechanised fillet weld is applied from the inside of the closed stiffener by equipment developed for this purpose; see Figure 4a. Figure 4b shows a photo of the resulting weld. Second, a steered arc welding process is available at several European construction companies, which enables full control and automatic feedback of

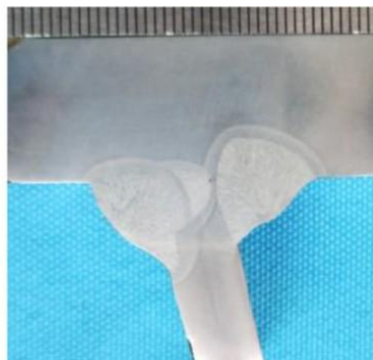
the welding parameters during the process. This weld process allows for a weld with controlled melt through, generating a constant geometry of the weld inside the closed stiffener that is fully fused with both the stiffener and the deck plate. Figure 5 provides a photo of the resulting weld. Both welding processes prevent unfused land present in the traditional single-sided welded connection, and thereby the requirements on h_1 and h_2 become obsolete. This can radically change the construction and fatigue performance of OBD-s. The benefits of these new welding processes over the traditional single-sided partial penetration welds are:

- Better reproducibility of the weld geometry, implying smaller variation of the weld geometry along the connection length and between connections. This is an advantage since fatigue is a weakest link failure mode.
- Less dependency of the distance between the stiffener web edge and the deck plate before and during welding, i.e., the measure h_1 (Figure 3) on the final geometry after completion of the weld.
- Absence of the lack of penetration (h_2 in Figure 3), which is a trigger for crack initiation because of the high stress concentration that it involves.

Obviously, the new welded connections could imply other locations of cracks, as indicated in Figure 6. The aim of this paper is to evaluate fatigue tests and conduct fracture



a) Fully mechanized weld inside the stiffener
Figure 4. Double-sided weld



b) Photo of the weld cross-section
(Figure reproduced from [16].)

mechanics simulations to estimate the lower bound fatigue resistance of the crack locations that could potentially occur in the new welded connections. These estimates can then be implemented in TS 1993-1-901. Section 2 explains the methods and models used to estimate the fatigue resistance. Section 3 provides the resulting fatigue resistances. Section 4 provides conclusions and recommendations.

2 Methods and models

This paper uses conventional techniques to estimate the fatigue resistance of the new welded connections shown in Figures 4 and 5. Section 2.1 explains how fatigue tests are evaluated to obtain a lower bound fatigue resistance. Section 2.2 explains the fracture mechanics model used. Section 2.3 explains how the *S-N* curves for TS 1993-1-901 are based on the analyses of Sections 2.1 and 2.2.

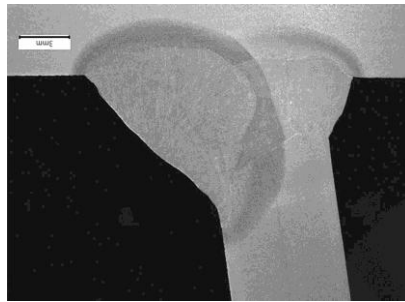


Figure 5. Single-sided welded connection with continuous and controlled melt through (weld and photo produced by construction company Hollandia Infra)

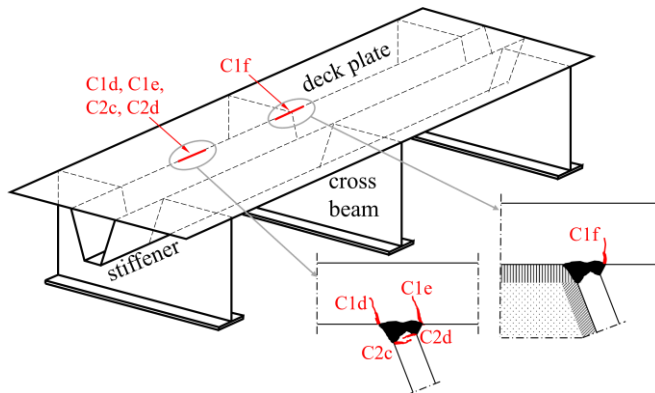
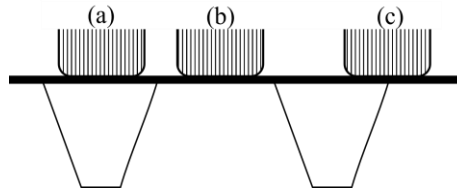


Figure 6. Orthotropic bridge deck with the five fatigue-sensitive details in the new (double-sided or continuous melt-through) stiffener-to-deck plate connections

2.1 *Derivation of lower bound fatigue resistance curves from tests*

Fatigue tests are collected from the literature. Fatigue tests are not available for the welded connection with controlled melt-through (Figure 5), but tests are available for the double-sided welded connection (Figure 4). The test data are collected based on the following criteria:

- Obviously, the welded connection should correspond to that of Figure 4 (Tests on the weld with controlled melt through are not available). It is assumed that the welds are of usual quality level for bridge decks, which is quality level B of ISO 5817 [17]. Photos of the specimens in the literature were evaluated to check the compliance with the requirements in [17] and to check consistency between the sources of, for example, weld size.
- The geometry should correspond to that in a realistic orthotropic bridge deck. In modern bridge decks, the deck plate thickness is 16 mm or thicker and the stiffener has a thickness from 6 to 8 mm. The deck should be supported in a realistic manner, i.e., the stiffeners provide support to the deck plate.
- Related to the previous item, the load should be realistic. A tyre of a heavy vehicle causes the deck plate to be loaded in bending, where the support by the stiffener causes compression at the bottom side of the deck at the welded connection (and tension at the top side of the deck). The tyre can be applied on any location on the deck, where crack types C1e and C1f are usually observed in tests with a tyre centred above the stiffener (Figure 7a) and crack type C1d is observed for a tyre centred between two stiffeners (Figure 7b), because of the higher stress levels at these sides of the connection. A complex loading condition results for the stiffener web, which is loaded by a combination of bending and compression. The largest stress range occurs for alternating loads at either side of the connection.
- The tests should be conducted with constant amplitude loading. Tyre loads are of variable amplitude nature, but constant amplitude loads are required to derive $S-N$ curves. It is not necessary to have a rolling wheel in the test; a hydraulic jack on a fixed position on the deck can exert the fluctuating load.



a) Centred above a stiffener b) Centred between two stiffeners c) Centred above a stiffener web

Figure 7. Wheel positions in transverse direction

Unfortunately, the number of tests satisfying the above requirements is too small to derive an $S-N$ curve. For this reason, the requirements are compromised, where Section 3 explains how non-conforming data are treated per detail.

Standards for fatigue verification adopt various stress definitions. The definition that is easiest to use in most applications is the nominal stress, which is the stress excluding the effects of the connections. In OBD-s, however, this stress is not well defined because the effects of connections cannot be excluded without over-simplifying the structure. For this reason, TS 1993-1-901 adopts the hot-spot stress method where possible, which is the stress extrapolated along the plate surface to the weld toe, following certain definitions [6]. Since the hot-spot stress differs from the nominal stress, the $S-N$ curve should also differ to achieve the same fatigue resistance. In line with TS 1993-1-901, the $S-N$ curves derived here are based on stresses obtained with the hot-spot stress approach.

In agreement with EN 1993-1-9 [5] and TS 1993-1-901 [4], the lower bound $S-N$ curve is defined as the prediction bound with a 95% exceedance probability. A Basquin equation is assumed for the fatigue test data:

$$\log_{10}(N) = C + m \log_{10} \frac{\Delta\sigma}{[MPa]} \quad (1)$$

where N is the number of cycles to failure and $\Delta\sigma$ is the constant amplitude stress range. Based on prior knowledge of other welded details, the $S-N$ curve slope parameter m is set to a predefined value of $m = -3$, but the appropriateness of this parameter is checked for each detail. Constant C is detail-dependent, and it is evaluated based on the collected fatigue tests. In this respect, all fatigue tests of the same detail but from different series and labs are pooled. Only failed data are included in the evaluation; run-outs are ignored. The

fatigue test data are assumed to be lognormally distributed, and a least squares method is applied to determine C . The characteristic reference fatigue resistance $\Delta\sigma_C$ of the S - N curve is the value on the curve at $N = 2 \cdot 10^6$ cycles:

$$\log_{10}(\Delta\sigma_C) = \frac{\log_{10}(2 \cdot 10^6) - \hat{C} + s_C t_{(0.95, n-1)} \sqrt{1 + 1/n}}{m} \quad (2)$$

where n is the number of available tests, $t_{(0.95, n-1)}$ is the inverse of Student's T distribution with 95% probability and $n - 1$ degrees of freedom, \hat{C} is the expectation of C , and s_C is its standard deviation estimated from the available tests:

$$\hat{C} = \frac{1}{n} \sum_{i=1}^n \log_{10}(N_i) - \frac{m}{n} \sum_{i=1}^n \log_{10}(\Delta\sigma_i) \quad (3)$$

$$s_C = \sqrt{\frac{1}{n-1} \sum_{i=1}^n (\log_{10}(N_i) - \hat{C} - m \log_{10}(\Delta\sigma_i))^2} \quad (4)$$

The term $t_{(0.95, n-1)} \sqrt{1 + 1/n}$ follows from a Bayesian estimate of C under limited available data [18]; see Figure 8. The above-mentioned procedure has been followed for all details in EN 1993-1-9 [5]; see [19].

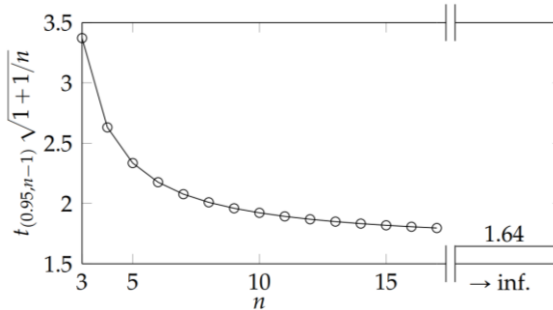


Figure 8. Multiplication factor of the standard deviation for a 95% prediction bound

2.2 Derivation of S - N curves from fracture mechanics

A linear elastic fracture mechanics simulation framework is employed to estimate the fatigue resistance and the effect of changes in certain geometric parameters on the fatigue resistance. The framework uses the Forman Mettu [20] (also referred to as Nasgrov [21]) crack growth relationship with the stress intensity factor (SIF) range for a Mode I crack, Δ_K , as the fatigue driving force:

$$\frac{da}{dN} = \begin{cases} 0 & \text{if } \Delta K \leq \Delta K_{th} \\ C_K \left(\frac{1-f_K}{1-R_K} \Delta K \right)^{m_K} \left(1 - \frac{\Delta K_{th}}{\Delta K} \right)^p & \text{if } \Delta K > \Delta K_{th} \end{cases} \quad (5)$$

where C_K , m_K and p are material parameters, R_K is the ratio of the stress intensity factor ($R_K = K_{\min} / K_{\max}$), and the threshold of the stress intensity factor ΔK_{th} and the crack opening factor f_K follow from:

$$\Delta K_{th} = \Delta K_0 \sqrt{\frac{a}{a+a_H} \left[\frac{(1-A_0)(1-R_K)}{1-f_K} \right]^{1+C_{th}R_K}} \quad (6)$$

$$f_K = \begin{cases} \max(R, A_0 + A_1 R_K + A_2 R_K^2 + A_3 R_K^3) & \text{if } R \geq 0 \\ \max(0, A_0 + A_1 R_K) & \text{if } -2 \leq R < 0 \\ \max(0, A_0 - 2A_1) & \text{if } R < -2 \end{cases} \quad (7)$$

$$A_0 = (0.825 - 0.34\alpha + 0.05\alpha^2) \cos^{1/\alpha} \left(\frac{\pi \Delta \sigma}{(1-R)(\sigma_y + \sigma_u)} \right) \quad (8)$$

$$A_1 = (0.415 - 0.071\alpha) \frac{2\Delta \sigma}{(1-R)(\sigma_y + \sigma_u)} \quad (9)$$

$$A_3 = 2A_0 + A_1 - 1 \quad (10)$$

$$A_2 = 1 - A_0 - A_1 - A_3 \quad (11)$$

where C_{th} and ΔK_0 are material parameters, a_H is El Haddad's correction to account for the difference in the threshold between short and long cracks [22], taken as 0.381 [23], and alpha is a plane stress versus plane strain correction factor with an assumed value of 2. The effect of the stress intensity factor ratio R_K in Eq. 5-6 is limited to a value R_{cl} . For $R_K > R_{cl}$ the crack may be assumed to be fully open, and the crack growth relationship applies as for $R_K = R_{cl}$. On the other hand, one should be cautious in using the relationship for very low R_K values because of a lack of test data. This study therefore uses R_K not lower than -3.

Material parameters C_K , m_K , p , ΔK_0 , C_{th} , and R_{cl} are based on data for steel grade ASTM A36 in [23]. This steel grade, comparable to the European grade S235, deviates from ASTM A572 Grade 50, the Chinese grade Q355 and the European grade S355 typically used for OBD-s. However, the parameters of the Forman-Mettu relationship for the latter steel grades are not available in textbooks. All of these steel grades are low alloy steels, and tests

conducted by the authors on S355 specimens gave similar crack growth rates to those on S235 specimens. The material parameters of A36 are, therefore, deemed representative of the steel grades used in OBDs. Data in [23] for various steel grades indicate that R_{cl} is independent of the steel grade.

Reference [23] provides expectations (mean values) for the material parameters. However, for consistency with the procedure of deriving the fatigue resistance from tests, the parameters C_K and ΔK_0 should be obtained for 5% and 95% exceedance probabilities, respectively. This study uses a coefficient of variation for C_K equal to 0.22, which is recommended for welds in [24], and a coefficient of variation for ΔK_0 equal to 0.15. The latter value is higher than the recommendation in [25]; see [26], because the author's experience is that the scatter in ΔK_0 is larger than this recommendation. Both variables are assumed to be log-normally distributed [26]. Table 1 provides the resulting material parameters, and Figure 9 presents the crack growth relationship for different stress ratios.

Table 1. Parameters of the crack growth relationship used in the analysis. Units: [N] and [mm]

ΔK_0	C_K	m_K	p	C_{th}	R_{cl}
Mean = 243	Mean = $6.05 \cdot 10^{-13}$	3	0.5	0.1 for $R < 0$	0.7
95% value = 190	5% value = $8.69 \cdot 10^{-13}$			2 for $R \geq 0$	

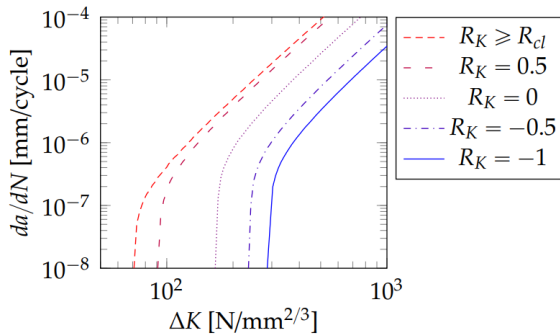


Figure 9. Crack growth relationship for different stress intensity factor ratios R_K

Application of the crack growth relationship requires the SIF range ΔK and its ratio R_K . The SIF range is determined by assuming a semi-elliptical surface crack at the weld toe; see Figure 10a. Strictly speaking, the transitions on the inner side of the single-sided welded

connection with controlled melt-through, at the onset of cracks C1e and C2d, are not weld toes. However, given the similarity of the geometry, they are treated as such. The crack growth is evaluated at the deepest point A and at the surface point C of the crack; see Figure 10a. The crack growth relationship in the width direction, dc/dN , is equal to Eq. 5, but the actual crack growth in the two points differs because of the different SIF ranges:

$$\Delta K_A = \left(M_{m,a} M_{km,a}^* + M_{b,a} M_{kb,a}^* \right) f_\theta f_\rho \Delta \sigma \sqrt{\pi a} \quad (12)$$

$$\Delta K_C = \left(M_{m,c} M_{km,c}^* + M_{b,c} M_{kb,c}^* \right) f_\theta f_\rho \Delta \sigma \sqrt{\pi a} \quad (13)$$

where

$$M_{km,a}^* = M_{km,a} f_{\rho m} \quad (14)$$

$$M_{kb,a}^* = M_{kb,a} f_{\rho b} \quad (15)$$

and similar equations for $M_{km,c}^*$ and $M_{kb,c}^*$. The classical solution of Newman and Raju [27] is adopted for the geometric correction factors accounting for the semi-elliptical crack subjected to membrane action $M_{m,a}$ and $M_{m,c}$, and bending $M_{b,a}$ and $M_{b,c}$. The solution of Bowness and Lee [28] is adopted for the geometric correction factors accounting for the presence of the weld for membrane action $M_{km,a}$ and $M_{km,c}$, and for bending $M_{kb,a}$ and $M_{kb,c}$. This solution is valid for a sharp transition at the weld toe ($\rho = 0$, see Figure 10a for

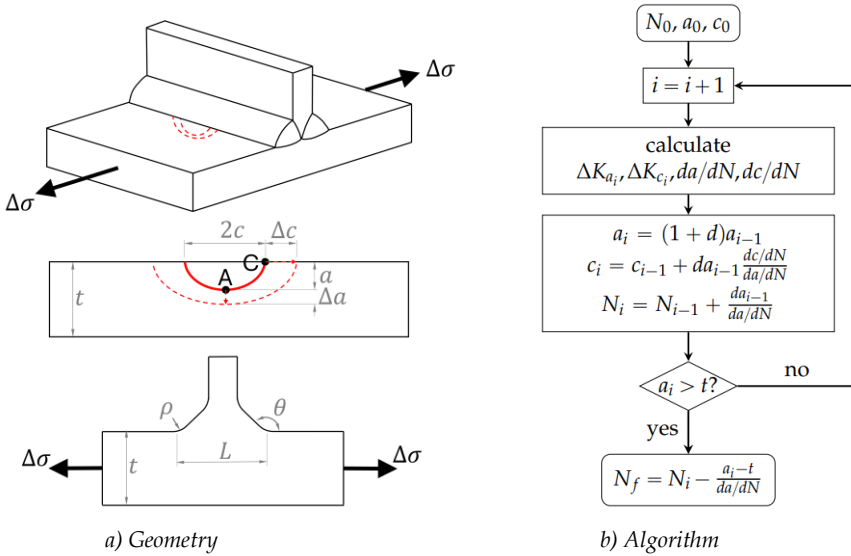


Figure 10. Principle of the classical fatigue fracture mechanics framework

the definition) and a weld toe angle $150^\circ \leq \theta \leq 115^\circ$. Given the small difference in factors for small weld toe angles, it is reasonable to consider the factors for $\theta = 115^\circ$ also valid for θ down to 90° . Bowness and Lee [28] have also provided geometric correction factors for welds with $\rho/t = 0.1$, but not for other weld toe radii. To account for weld toe transitions with $\rho > 0$, the geometric correction factors f_ρ of Dijkstra et al. [29] are therefore adopted. These factors are valid for $0 \leq \rho/t \leq 1.25$. They were originally developed for the M_k factors of [30] instead of [28], but they have been verified to produce similar effects on the fatigue life of the weld toe transition for the two solutions of the M_k factors. The geometric correction factors M and M_k are functions of both crack depth a and semi crack length c , whereas f_ρ only depends on a . A value of 0.15 mm is used for a in calculating f_ρ for the surface point C of the crack.

The geometrical correction factors M_k are derived for connections involving two perpendicular plates, whereas the stiffener web is inclined to the deck plate, often at an angle of 60° to 70° . However, this angle has a negligible effect on the stress distribution in the deck plate near the weld toe. The model is therefore deemed appropriate for the evaluation of Details C1d, C1e, C2c, and C2d. The geometrical correction factors M_k are derived for the nominal stress method. If the verification is based on the hot-spot stress range, as intended here, BS 7910 [25] states that the geometrical correction factors M_k can be approximated with a modified distance between the weld toes, maximized by the semi-thickness of the stressed plate, i.e., $L = 0.5 t$. This approximation is adopted in the current study.

Because of the presence of the crossbeam web, a complex stress distribution follows for Details C1c and C1f. Geometrical correction factors for C1c are developed in [31]. This model is not applicable to Detail C1f. A modified factor $M_{kb,c}^m$ is defined for this detail, based on [32], that accounts for the decaying influence of the crossbeam as the crack grows in the width direction. This results in a reduction of hot-spot stress at the surface point C. Factor $M_{kb,c}^*$ is defined as.

$$M_{kb,c}^m = r_c M_{kb,c}^* \quad (16)$$

$$r_c = g + (1 - g) \cos \frac{\pi c}{h + c} \quad (17)$$

where r_c accounts for the decaying hot-spot stress, and g and h are calibration parameters

that account for the magnitude of reduction of the hot-spot stress and the distance over which this reduction takes place.

The ratio of the stress intensity factor $R_K = K_{\min}/K_{\max}$ depends on the applied load and the residual stress:

$$R_K = \frac{\frac{R\Delta K}{1-R} + K_{\text{res}}}{\frac{\Delta K}{1-R} + K_{\text{res}}} \quad (18)$$

where $R = \sigma_{\min}/\sigma_{\max}$ is the ratio of the applied load, and K_{res} is the stress intensity factor due to the residual stress. For a transverse attachment in the depth direction (A):

$$K_{\text{res},a} = M_{m,a} \sigma_{\text{res}} \left(1 - \frac{a}{t}\right) \sqrt{\pi a} \quad (19)$$

and in the width direction (C):

$$K_{\text{res},c} = M_{m,c} \sigma_{\text{res}} \sqrt{\pi a} \quad (20)$$

where σ_{res} is the residual stress at the plate surface, transverse to the weld direction. It is estimated from finite element analyzes and, in some cases, measurements presented in the literature, i.e., [33, 34, 35, 36] for the double-sided welded connection and [37, 38, 39] and [37, 38, 40] for the weld toe and the weld root, respectively, of the traditional single-sided partial penetration welded connection. The simulations provide a residual stress at the weld toes of up to approximately 250 MPa, i.e., 2/3 of the nominal yield stress of the applied steel grades. These values agree with those of normal transverse attachments [41]. Residual stress data are not available for the single-sided welded connection with controlled melt through, nor for the stiffener-to-deck plate welded connection at the crossbeam location. The influence on fatigue resistance is therefore determined for some of the details by varying the residual stress by 25%. The factor $(1 - a/t)$ in Eq. 19 represents the decay of residual stress in the depth direction, and it is taken from BS 7910 [25] for a transverse attachment, as per Figure 10a.

A framework is set up where, starting from initial dimensions a_0 and c_0 , a crack is extended incrementally in the depth direction by a factor da up to the attainment of a final crack depth $a = t$, where d is taken as 10^{-3} , and the associated number of cycles and extension in the width direction are determined; see Figure 10b. The simulation starts with

an initial crack with a size of $a_0 = 0.15$ mm and $a_0/c_0 = 0.62$, as recommended in the JCSS probabilistic model code [18], which are the mean values obtained from measurements on a large steel structure [42]. Other dimensions vary by detail and will be given in Section 3.

As a (partial) validation of the fracture mechanics model, the hot-spot $S-N$ curve of a transverse attachment as per Figure 10a is predicted with the model and compared to the curve in EN 1993-1-9 [5], the latter providing $\Delta\sigma_C = 100$ MPa. The geometric dimensions selected for this purpose are $t = 15$ mm and $\theta = 45^\circ$, while ρ is varied between 0 and 2 mm. The applied stress ratio is $R = 0.1$. Figure 11a gives the results. The $S-N$ curves agree reasonably for $\rho \approx 1$ or 2 mm. The same analysis is conducted for the nominal stress method. In this case, the node length L (Figure 10a) is an input variable, for which a value $L = 2t$ is selected – representing a transverse attachment thickness of 10 mm and weld throats of 4 mm. The results in Figure 11b indicate that the $S-N$ curve of the fracture mechanics analysis agrees well with that of the standard ($\Delta\sigma_C = 80$ MPa) for $\rho = 1$. Such a rounding radius also seems a reasonable lower bound estimate for weld toes in steel structures. The curved crack growth relationship of Eq. 5 causes a slight curvature of the predicted $S-N$ curve towards the “constant amplitude fatigue limit” (actually the transition to the very high cycle fatigue stage). This curvature is realistic, as it is also often experienced in fatigue tests [43].

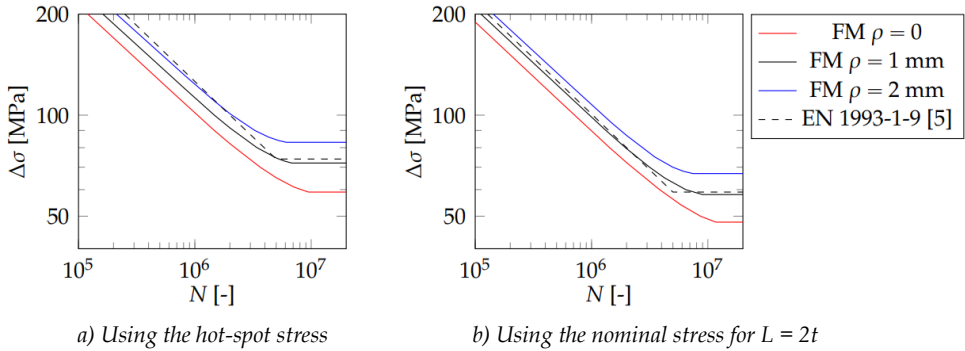


Figure 11. Simulation of the $S-N$ curve for a transverse attachment using the fracture mechanics (FM) model and the $S-N$ curve of EN 1993-1-9 [5]

2.3 FAT classes

Standards such as EN 1993-1-9 [5] provide a limited, predefined number of $S-N$ curves. These curves are characterised by their so-called detail category or FAT class. The FAT

class is represented by a number that equals the fatigue resistance $\Delta\sigma_C$ in MPa (the FAT class is unitless). By convention, the FAT class of a given detail is obtained by rounding down $\Delta\sigma_C$ resulting from the tests to one of the predefined FAT classes. In this study, the same approach is followed if $\Delta\sigma_C$ is obtained from the fracture mechanics method instead of the tests.

3 Results – Fatigue resistance

3.1 Detail C1d

No significant difference is expected between the fatigue resistance of Detail C1a of the traditional single-sided welded connection and that of Detail C1d of the new welded connections as shown in Figure 12, because the connection is unaltered at the initiation site of these crack types. Test data are collected to verify this hypothesis.

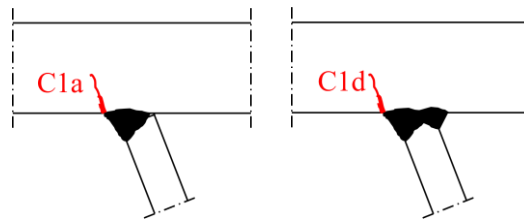


Figure 12. Graphics of Details C1a and C1d

Table 2 presents the test series found in the literature on the double-sided welds where cracks of Type C1d developed. In this table, n_f and n_r stand for the number of failed tests and run-outs, respectively. The fluctuating load was applied on a rubber patch between the two stiffeners in all tests in [44] and in some of the tests in [45]. Other tests in [45] were conducted with the load centered above the stiffener. All specimens, except for one, failed according to Detail C1d. In both set-ups, the deck plate was supported at its edges, whereas the stiffeners were unsupported, resulting in the stiffener webs acting as transverse stiffeners. This set-up causes a sagging bending moment in the deck plate at the weld location, with tension at its bottom side, whereas a hogging bending moment with

Table 2. Test series of Detail C1d with stress ratio $R = 0$

Source	t_d	t_s	n_f	n_r	Remark
Zhu et al. [44]	18	8	7	0	Stress from strain at 5 mm from weld toe
You et al. [45]	18	8	2	3	Stress from strain at 10 mm from weld toe

compression at the weld location occurs in OBDs, caused by the support exerted by the stiffeners. This results in a difference in the mean stress of the cycle.

Tests with the traditional single-sided partial penetration weld have demonstrated that the mean stress has a significant influence on the fatigue resistance of the comparable Detail C1a [7]. For this reason, the tests in [44] cannot be directly used to determine fatigue resistance. Instead, the results of the tests in [44] on Detail C1d are compared with those collected on Detail C1a, which has a similar stress ratio of $R \approx 0$. If the data for these two details agree for $R \approx 0$, they are deemed to also agree for negative or zero mean stress.

The stresses in the tests of [44] and [45] are obtained from a strain gauge attached to the bottom side of the deck plate at distances of 5 mm and 10 mm, respectively, from the weld toe, assuming unidirectional stress and the Young's modulus. The hot-spot stress might be slightly larger, but given the specimen geometry, the difference is expected to be insignificant.

Figure 13 provides the collected data of Details C1d and C1a with $R \approx 0$. Symbol p_r in the legend refers to the penetration ratio of the traditional single-sided welded connection. Run-outs are not displayed to enhance the readability of the figure. Assuming slope parameter $m = -3$, the fatigue resistance of all series is similar, except for Series C1a [11] $p_r = 80\%$. Some data in this series show a significantly higher resistance compared to all other series. The reason for the deviation is unknown. Excluding this series, the fatigue resistance of the entire datapool appears equal to that of Detail C1d only, and it is $\Delta\sigma_C = 111$ MPa.

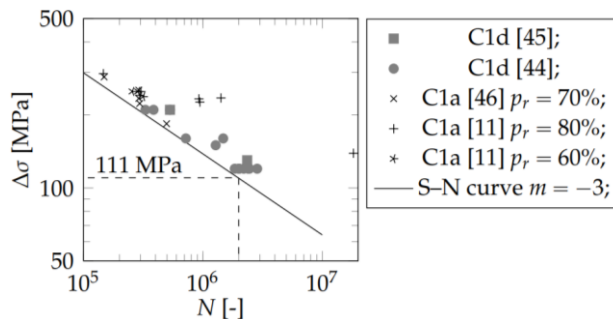


Figure 13. Fatigue test data for Details C1d and C1a with $R \approx 0$

The data in [44] displayed in Figure 13 represent double-sided welds. Ocel [11] and Yuan [47] conducted tests with stiffener-to-deck plate welds made from one side, predominantly with a partial penetration weld but some with melt-through. The extent of the melt-through and the fusion condition are unknown. Most tests failed through a crack growing from the weld toe into the deck plate (Detail C1a in Figure 1). In these, the tests with melt-through provided lower resistance compared to the tests with partial penetration welds. However, [11] and [47] attributed this to the relatively small dimensions of the weld resulting from the weld process applied to the specimens with melt-through. TS 1993-1-901 therefore provides requirements on dimensions h_3 and h_4 (Figure 3). Further, the geometric transition between the weld toe and the deck plate must be smooth. These requirements apply to Detail C1a and the same requirements are proposed for Detail C1d, see Figure 14 for the symbol explanation.

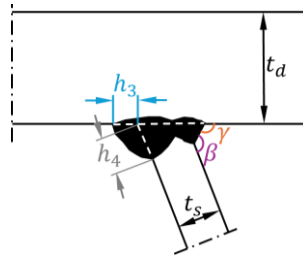


Figure 14. Dimensional parameters of the new welded connections

The fatigue resistance of Detail C1a with a stress ratio of $R = -1$ determined in [7] is $\Delta\sigma_C = 153$ MPa for deck plates with $t_d \leq 14$ mm thickness. A fracture mechanics model is conducted with the following variables: $t_d = 14$ mm, $\theta = 135^\circ$, $\rho = 2$ mm, $R = -1$. The resulting fatigue resistance is $\Delta\sigma_C = 164$ MPa. The fracture mechanics model provides a perfect match with the resistance according to the tests for a (calibrated) weld toe radius of $\rho = 1.5$ mm. The model predicts a 6% lower resistance for a deck plate thickness of $t_d = 20$ mm. The FAT class of Detail C1a is set to 140 for $t_d \leq 14$ mm and FAT class 125 of $t_d > 14$ [7]. The parameters of the fracture mechanics model of Detail C1d are the same as those of Detail C1a. Based on the test data and considerations presented above, the same FAT classes are proposed for Detail C1d.

3.2 Detail C1e

Main attention in this study is devoted to Detail C1e because of the sensitivity to the local connection geometry of the corresponding Detail C1b of the traditional, single-sided partial penetration weld, see Figure 15.

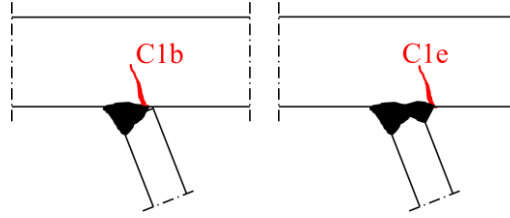


Figure 15. Graphics of Details C1b and C1e

Table 3 gives the test series found in literature on the double-sided welds where cracks of Type C1e developed. The tests of [36] are not considered in the analysis because the bolts used in the test set-up to clamp the specimen are expected to result in a stress concentration at the weld, whereas this is not accounted for in the reported stress. Hence, [36] may have underestimated the stress.

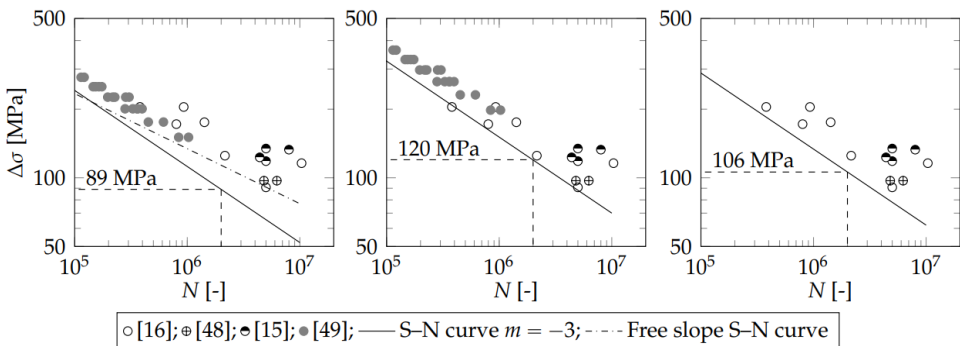
Table 3. Test series of Detail C1e with stress ratio $R = -1$

Source	t_d	t_s	n_f	n_r	Remark
Cui et al. [16]	16	8	7	0	3 specimens with non-constant load range.
Chen et al. [48]	16	8	2	0	
Zhang et al. [15]	18	8	4	2	Stress from strain at t_d from weld toe.
He et al. [36]	14	8	2	0	Stress possibly underestimated.
Yang et al. [49]	16	7	20	0	Nominal stress. Tests executed in tension.
					External load ratio $R_{ext} = 0.1$ and 0.5 .

The stress range of all series except for [48] needs to be modified to be representative of the hot-spot stress in an OBD. The stress in [15] and [49] was determined from strain gauges attached to the bottom side of the deck plate at a certain distance from the weld toe. Based on a finite element analysis with solid elements in [48], the read-out stress is converted to the hot-spot stress in these cases through multiplication with a factor of 1.09. Three of the tests in [16] were carried out with different blocks of constant amplitude load, where the amplitude increased in subsequent blocks. Deviating from [16], the current paper considered only the last block and associated number of cycles in the evaluation. Hence, it is conservatively assumed here that prior blocks did not induce damage. The tests of [49] were carried out in tension, whereas the detail in orthotropic bridge decks is loaded in bending. This has two consequences:

- A stress gradient over the deck plate thickness occurs in case of bending in real decks with compression at the deck plate bottom side (where the weld is located), resulting in slower crack growth compared to tension.
- The specimens contained angular misalignment. This has no consequences for the local stress in a specimen subjected to bending, but it causes a local stress increase in the tension specimens.

To account for the misalignment influence, [49] used simple correction factors to enhance the fatigue resistance. This factor is 1.15 on average. The fracture mechanics model explained in Section 2.2 is used here to account for the difference between tension load with $R = 0.1$ or 0.5 and bending load with $R = -1$. It results in a fatigue resistance enhancement factor of 1.3. Both factors are substantial, however, they are based on structural models involving uncertainty by definition. Therefore, the regression analysis is conducted with different treatments of the enhancement factors, see Figure 16. Figure 16a gives the S - N curve using all test data (except for those in [36]), transferred to the hot-spot stress where necessary, and using the enhancement factor for misalignment of the tests of [49], but ignoring the enhancement factor for bending and load ratio. Figure 16b gives the same data but including the enhancement factor for bending and load ratio for the tests in [49]. Figure 16c gives the test data without those of [49]. The resulting fatigue resistances of the three subfigures are $\Delta\sigma_C = 89$ MPa, 120 MPa, and 106 MPa, respectively. The former value is evidently too low because no correction is applied on the tensile load application of the tests in [49].



a) All data as received

b) Data in [49] converted to bending loading based on LEFM

c) Excluding data in [49]

Figure 16. Fatigue test data for Detail C1e, with the stress converted to hot-spot stress

The fracture mechanics model used to estimate the fatigue resistance has the following variables: $t_d = 18$ mm, $\rho = 0$ mm, $\gamma = 125^\circ$, and $R = -1$ MPa. Values of ρ and γ are based on cross-sectional photos of the double-sided welded connection in [15, 16, 34, 48, 50, 51, 52]. The fracture mechanics model predicts a fatigue resistance of $\Delta\sigma_C = 112$ MPa, i.e., in agreement with the regression value of the tests.

Fatigue test data of the welded connection with controlled melt-through do not yet exist. There are two potential differences between this welded connection and the double-sided welded connection that may affect the fatigue resistance:

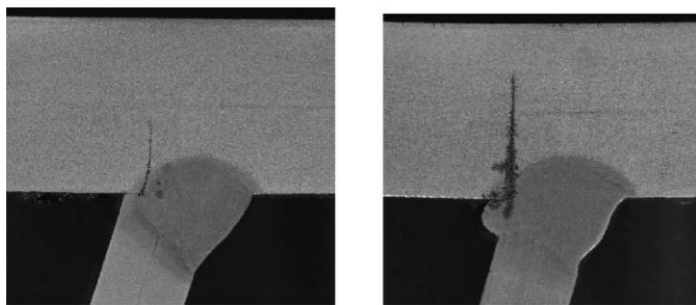
- The weld toe angle of the single-sided welded connection with controlled melt through is $\gamma \approx 90^\circ$ whereas that of the double-sided welded connection is $\gamma \approx 135^\circ$.
- The residual stress may differ between the two weld processes.

The effect of the former aspect is studied using the fracture mechanics model. It results in a marginal reduction of the single-sided welded connection with controlled melt-through of 4% compared to the double-sided welded connection. This marginal effect is confirmed with the test results in [49], where double-sided welds with different flank angles are tested, without a significant effect on the fatigue performance. The residual stress resulting from the double-sided weld process appears significant, as given above. The residual stress resulting from the process with controlled melt-through is unknown but expected to be high as well. The fracture mechanics model predicts a variation of 4% in the fatigue resistance for an assumed variation in residual stress of 25%. This is confirmed with the test results in [49], where the tests with $R = 0.1$ and the tests with $R = 0.5$ give similar results. For these reasons, equal FAT classes of the two processes are proposed. A FAT class of 100 is proposed for Detail C1e, which is a lower bound of the tests and the fracture mechanics simulations and, therefore, possibly conservative.

Ya et al. [53] tested specimens with the traditional single-sided welds with 80% penetration and also specimens with uncontrolled melt-through. The latter specimens had a non-constant penetration ratio and inconsistent fusion of the weld metal with the deck plate, see Figure 17. The tests with uncontrolled melt-through gave a lower fatigue resistance, see Figure 18. The proposed FAT class of 100 would be too high for the latter test data ($\Delta\sigma_C =$

88 MPa). This implies that full control of melt-through – resulting in a constant shape of the weld profile and full fusion of the weld metal with the deck plate inside the stiffener – is considered crucial for a good performance of Detail C1e.

The geometrical requirements on Detail C1e for the FAT class to be valid are specified in agreement with the parameters of the fracture mechanics analysis and the photos of the realized welds of both new weld processes. This results in $\gamma \leq 90^\circ$, see Figure 14, and no requirement on the smoothness of the weld toe transition (i.e., any value of ρ is allowed).



a) 80% penetration weld

b) Uncontrolled weld melt through.

Figure 17. Cracks of tested details in [53] (Figure reproduced from [53].)

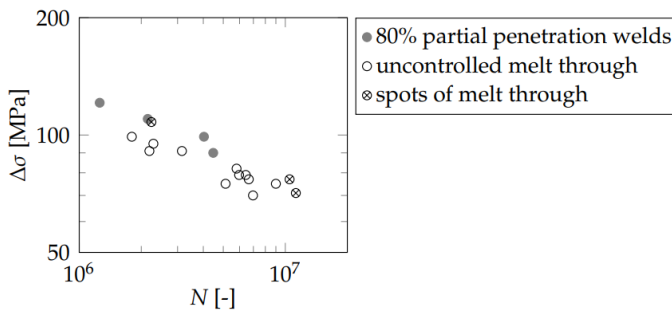


Figure 18. Test data by Ya et al. [53] for $R = 0.2$

3.3 Detail C1f

The global stress distribution of Detail C1f is similar to that of Detail C1c (Figure 19): The presence of the crossbeam results in a high stress concentration in case of loading by a tyre above the stiffener, but the stress reduces with distance from the crossbeam. This causes a relatively low crack growth rate or even crack arrest. Different from all other details, these

details are not loaded if the tyre is located between two stiffeners. Further, Detail C1c is deemed less sensitive to the local weld geometry compared to Detail C1b because:

- The stiffener-to-deck plate weld is applied before the crossbeam web-to-deck plate and crossbeam web-to-stiffener welds. Shrinkage of the latter weld is expected to cause the stiffener and the deck plate to not be in contact, i.e., $h_1 > 0$ for the traditional single-sided partial penetration welded connection.
- Simulations with the finite element method show that the effective notch stress is insensitive to the penetration ratio in the studied range $0 \leq h_2 \leq 1.5$ mm [54, 55].

Only one test series is available for evaluating the fatigue performance of Detail C1f [15]. The series contains two tests with the double-sided welded connection and two tests with the traditional single-sided, partial penetration welded connection. These tests are performed on full-scale mock-ups of an OBD with $t_d = 18$ mm, $t_s = 8$ mm, and a crossbeam web thickness of $t_c = 14$ mm.

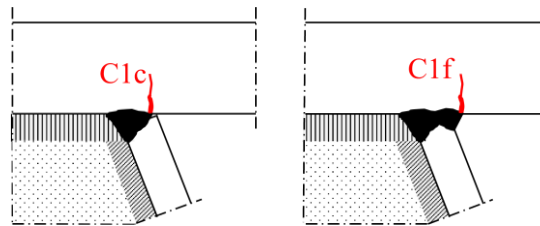


Figure 19. Graphics of Details C1c and C1f

Table 4 provides the results, where N_{25} refers to the number of cycles in which the strain range measured close to the crack initiation point changed by 25%. The loads applied are higher on the double-sided welded connections, whereas their average fatigue life is also higher. This suggests that the double-sided welded connections perform better in fatigue than the traditional single-sided partial penetration welded connections for this detail. However, the number of tests is insufficient for a definitive conclusion.

Table 4. Fatigue test data in [15] on Details C1c and C1f

Connection	Detail	Load [kN]	N_{25}
partial penetration	C1c	150	960 000
partial penetration	C1c	150	780 000
double-sided	C1f	180	840 000
double-sided	C1f	180	1 300 000

A fracture mechanics simulation is conducted on Detail C1f with the following parameters: $t_d = 12$ mm, $\rho = 0$ mm, $\gamma = 90^\circ$, $g = 0.67$, $h = 24.5$ mm, and $R = -3$. Parameters g and h are taken from [31]. They are derived for Detail C1c, but the hot-spot stress is designed to be unaffected by the weld profile; hence, the parameters are deemed valid for Detail C1f. Because reference [31] used $t_d = 12$ mm, the same thickness is adopted here, although deck plates of modern bridge decks are often 18 mm or thicker. The simulation results in $\Delta\sigma_C = 177$ MPa. This value is 7.5% lower for a 25% higher residual stress ($\sigma_{res} = 310$ MPa). As a comparison, the fatigue resistance of Detail C1c, determined from tests on deck plates with $t_d = 12$ mm, is 170 MPa [7]. Thicker deck plates provide higher fatigue resistance for the comparable Detail C1c [7]. It is unknown whether this also applies to Detail C1f.

Based on the simulations and the tests, the fatigue resistance of Detail C1f is probably higher than that of Detail C1c; however, the number of tests is too small for a quantitative analysis. For this reason, the FAT class of C1f is conservatively taken to be equal to that of C1c: 170 for $t_d \leq 14$ mm, 190 for 14 mm, $< t_d < 18$ mm, and 200 for $t_d \geq 18$ mm. The constant amplitude fatigue limits are 93 MPa, 82 MPa, and 69 MPa, respectively, corresponding to 20, 25, and 30 million cycles. The reason for the relatively large number of cycles at the knee-point is explained in [7]. Experience with the design of OBDs according to TS 1993-1-901 [4] is that Detail C1c is (one of) the detail(s) driving the design of the deck plate thickness. For this reason, aiming for a more optimized FAT class, it is recommended to conduct more tests on Detail C1f.

3.4 Detail C2c

Similar to Details C1a and C1d, no significant difference is expected between the fatigue resistance of Detail C2a of the traditional single-sided welded connection and that of Detail C2c of the new welded connections (see Figure 20), because the connection is unaltered at the initiation site of these crack types.

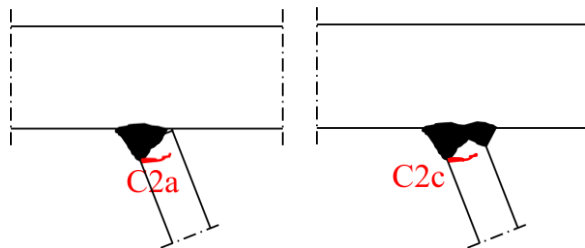


Figure 20. Graphics of Details C2a and C2c

Almost all fatigue tests conducted with the double welded connection resulted in either a crack in Detail C1d, C1e, or C1f, or in a run-out. As far as the authors could trace, one failure in the stiffener web occurred in the tests collected from the previous sections. These tests were conducted on OBDs or details thereof with realistic geometries, dimensions, and loading. This implies that an accurate estimate of the fatigue resistance of Detail C2c (and that of C2d) is less important than that of Details C1d, C1e, and C1f.

Tests on the comparable Detail C2a in [7] conducted with pure bending and $R = -1$ gave $\Delta\sigma_C = 159$ MPa, rounded to the nearest FAT class of 160. A fracture mechanics simulation is conducted with the following parameters: $t_s = 8$ mm, $\beta = 135^\circ$, $\rho = 1$ mm (equal to the limit of the application range of f_0) and $R = -1$. The simulation results in fatigue resistance of $\Delta\sigma_C = 155$ MPa. In realistic applications, the detail may not only be subject to cyclic bending but may also be subject to cyclic compression. For this reason, the simulations are repeated with an assumed ratio between membrane and bending stress of 1:1 and a stress ratio of $R = -3$ (equal to the limit of the application range of the crack growth relationship). A 6% lower fatigue resistance then results.

The same FAT class with the same prerequisite is proposed for Detail C2c as for Detail C2a. The prerequisite for the high DC is a smooth geometric transition between the weld and the stiffener web.

3.5 *Detail C2d*

The geometry of Detail C2d of the new welded connections is incomparable to that of Detail C2b of the single-sided welded connection with partial penetration; see Figure 21. Whereas Detail C2b represents a crack initiating from the root of the weld and growing through the weld, the crack of Detail C2d starts at the weld toe of the double-sided welded connection or the 'apparent' weld toe of the welded connection with controlled melt-through, and it grows through the stiffener web.

The geometry of Detail C2d shows a better resemblance to Detail C2c, but it has a steeper weld toe angle and a sharper transition at the weld toe. In the absence of test data, a fracture mechanics simulation is conducted with the following parameters: $t_s = 8$ mm, $\rho = 0$, $\beta = 135^\circ$ and $R = -1$. The simulation results in a fatigue resistance of $\Delta\sigma_C = 130$ MPa. A simulation with an assumed ratio between membrane and bending stress of 1:1 and $R = -3$

gives $\Delta\sigma_C = 129$ MPa. This is rounded down to the nearest FAT class of 125. The associated geometric requirements are $\beta > 135^\circ$, and there are no requirements on the smoothness of the weld toe transition (i.e., any value of ρ).

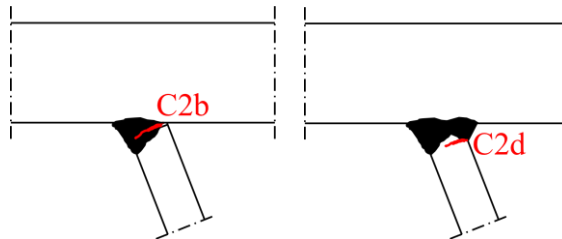


Figure 21. Graphics of Details C2b and C2d

4 Conclusions and recommendations

The welded connection between the stiffener and the deck plate in orthotropic bridge decks is a fatigue-sensitive detail. In order to overcome the drawbacks of traditional single-sided welded connections with partial penetration, two new welded connections are studied in this paper. The new welded connections comprise:

- A double-sided welded connection, where the weld applied from the exterior of the stiffener is followed by an automatic weld applied in the stiffener. This welded connection was first described by Japanese researchers and further studied and applied by Chinese researchers.
- A single-sided weld with controlled melt-through, creating a fully fused weld with continuous geometry at the inside of the stiffener. The weld process resulting in this geometry is available at a number of European construction companies.

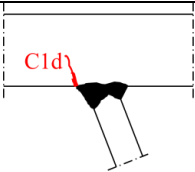
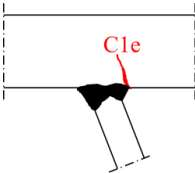
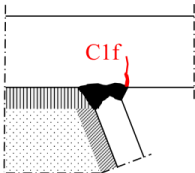
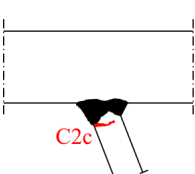
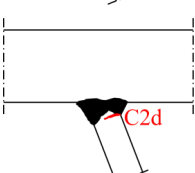
These new welded connections have the following advantages over the traditional single-sided partial penetration welded connection:

- Better reproducibility of the weld geometry, implying smaller variation of the weld geometry along the connection length and between connections. This is an advantage since fatigue is a weakest link failure mode.

- Less dependency of the distance between the stiffener web edge and the deck plate before and during welding, i.e., the measure h_1 (Figure 3) on the final geometry after completion of the weld.
- Absence of the lack of penetration (h_2 in Figure 3), which is a trigger for crack initiation because of the high stress concentration that it involves.

This paper presents test data and fracture mechanics analyses to estimate the fatigue resistance of the fatigue-sensitive details of the new welded connection. Table 5 provides the proposed FAT classes for stress ranges obtained using the hot-spot stress method based on these analyses. It also provides the associated requirements for the geometry.

Table 5. Summary of the proposed FAT classes for the hot-spot stress method

Detail	Graphic	FAT class	Requirements (Figure 14)
C1d		140 for $f_d \leq 14$ mm 125 for $f_d > 14$ mm	$h_3 \geq t_s$ and $h_4 \geq t_s$ and smooth weld toe transition
C1e		100	$\gamma \geq 90^\circ$
C1f		170 for $f_d \leq 14$ mm 190 for $14 \text{ mm} < f_d < 18 \text{ mm}$ 200 for $f_d \geq 18$ mm	$\gamma \geq 90^\circ$
C2c		160	$\beta \geq 135^\circ$ and $h_3 \geq t_s$ and $h_4 \geq t_s$
C2d		125	$\beta \geq 135^\circ$ and smooth weld toe transition

The number of available fatigue tests is small for some of the details. Detail C1f is one of the decisive details for the dimension of the deck plate. The FAT class of this detail is conservatively taken equal to that of Detail C1c. It is recommended that more tests be conducted on this detail.

Acknowledgments

The Dutch road authority Rijkswaterstaat is acknowledged for sponsoring this study. Frank van Dooren is acknowledged for the useful discussions and feedback on this study.

References

- [1] R. Wolchuk, Lessons from weld cracks in orthotropic decks on three European bridges, *Journal of Structural Engineering* 116 (1990) 75–84.
- [2] F. D. Jong, *Renovation techniques for fatigue cracked orthotropic steel bridge decks*, Doctoral thesis, Delft University of Technology (2007).
- [3] Q. Zhang, Y. Bu, Q. Li, Review on fatigue problems of orthotropic steel bridge deck, *China Journal of Highway and Transport* 30 (3) (2017) 14–30.
- [4] TS 1993-1-901, Fatigue design of orthotropic bridge decks with the hot spot stress method (final draft), CEN, 2023.
- [5] EN 1993-1-9 + C2, Eurocode 3: Design of steel structures – Part 1-9: Fatigue, CEN, 2009.
- [6] A. Hobbacher, *Recommendations for fatigue design of welded joints and components*, Springer, 2016.
- [7] J. Maljaars, R. Pijpers, W. Wu, H. Kolstein, Fatigue resistance of rib to deck, crossbeam to deck and deck to deck welds in orthotropic decks using structural stress, *International Journal of Fatigue* 175 (2023) 107742.
- [8] J. Hensel, T. Nitschke-Pagel, K. Dilger, Engineering model for the quantitative consideration stresses in fatigue design of welded components, *Weld World* 61 (2017) 997–1002.
- [9] Y. Liu, F. Chen, D. Wang, N. Lu, Fatigue crack growth behavior of rib-to-deck double sided welded joints of orthotropic steel decks, *Adv Struct Eng* 24 (3) (2021) 556–569.

- [10] C. M. Sonsino, T. Bruder, J. Baumgartner, S-N lines for welded thin joints – Suggested slopes and FAT values for applying the notch stress concept with various reference radii, *Weld World* 54 (2010) R375–R392.
- [11] J. Ocel, B. Cross, W. Wright, H. Yuan, Optimization of rib-to-deck welds for steel orthotropic bridge decks, Tech. rep., Federal Highway Administration – US Department of Transportation (2017).
- [12] N. Kanjo, H. Sugiyama, Y. Agano, S. Fujihira, M. Okumura, N. Okubo, Y. Natsuakim, Welding procedure test of inner fillet welding set for high durable orthotropic steel deck with trough rib, in: 66th Annual Academic Lecture Summary of Civil Engineering Society, 2011.
- [13] Q. Zhang, Y. Guo, J. Li, D. Yuan, Y. Bu, Fatigue crack propagation characteristics of double-sided welded joints between steel bridge decks and longitudinal ribs, *China Journal of Highway Transport* 32 (2019) 49–56.
- [14] Q. Zhang, D. Yuan, B. Wang, R. Han, J. Li, Fatigue performance of innovative both side welded rib-to-deck joints, *China Journal of Highway Transport* 33 (2020) 79–91.
- [15] Q.-H. Zhang, J. Li, D. Yuan, J. Z. Zhu, C. Cui, Fatigue model tests of orthotropic steel bridge deck of shenzhen-zhongshan link, *China Civil Engineering Journal* (2020).
- [16] C. Cui, Y. Ma, Q. hua Zhang, L. tian Da, S. hui Han, Fatigue strength and crack growth of double-side welded rib-to-deck joint in orthotropic steel decks, *Journal of Constructional Steel Research* 0 (2020) 107444.
- [17] ISO 5817, Welding – Fusion-welded joints in steel, nickel, titanium and their alloys (beam welding excluded) – Quality levels for imperfections, CEN, 2023.
- [18] JCSS, Probabilistic model code, JCSS, 2002. URL <https://www.jcss-lc.org/jcss-probabilistic-model-code/>
- [19] H. Bartsch, K. Drebenstedt, B. Seyfried, M. Feldmann, U. Kuhlmann, T. Ummenhofer, Analysis of fatigue test data to reassess EN 1993-1-9 detail categories, *Steel Constr* 13 (4) (2020) 280–293.
- [20] R. G. Forman, S. R. Mettu, Behavior of surface and corner cracks subjected to tensile and bending loads in ti-6al-4v alloy, Tech. rep., NASA (1990).
- [21] S. Mettu, V. Shivakumar, J. Beek, F. Yeh, L. Williams, R. Forman, J. McMahon, J. Newman Jr, Nasgro 3.0: A software for analyzing aging aircraft, in: *The Second Joint NASA/FAA/DoD Conference on Aging Aircraft*, 1999.
- [22] S. K. El Haddad M, Topper T, Prediction of non-propagating cracks, *Engineering Fracture Mechanics* 11 (1979) 573–584.

- [23] c. M. Ko S. Webster, J. Janosch, R. Ainsworth, R. Koers, FITNET Fitness-for-Service, FITNET Thematic Network/GKSS Research Centres Geesthacht, 2001.
- [24] DNV-RP-C210, Probabilistic methods for planning of inspection for fatigue cracks in offshore structures, Det Norske Veritas, 2019.
- [25] BS7910:2019, Guide to methods for assessing the acceptability of flaws in metallic structures, BSI, 2019.
- [26] J. Maljaars, J. Leander, A. Nussbaumer, J. D. Sørensen, D. Straub, Models and methods for probabilistic safety assessment of steel structures subject to fatigue, *Structural Safety* 113 (2025) 102446.
- [27] J. Newman, I. Raju, Stress intensity factor equations for cracks in three-dimensional finite bodies subjected to tension and bending, Technical Memorandum 83200, Tech. rep., NASA (1981).
- [28] D. Bowness, M. Lee, Fracture mechanics assessment of fatigue cracks in offshore tubular structures, Tech. rep., HSE Offshore Technology Report 2000/077 (2002).
- [29] O. Dijkstra, H. Snijder, I. VanStraalen, Fatigue crack growth calculations using stress intensity factors for weld toe geometries, in: *Proc. 8th Int. Conf. Offshore Mechanics and Arctic Engineering*, OMAE, 1989, pp. 137–143.
- [30] S. Maddox, R. Andrews, Stress intensity factors for weld toe cracks, in: *Proc. Computer aided assessment and control of localized damage*, 1990, pp. 329–342.
- [31] J. Maljaars, E. Bonet, R. Pijpers, Fatigue resistance of the deck plate in steel orthotropic deck structures, *Eng Fract Mech* 201 (2018) 214–218.
- [32] J. Maljaars, F. van Dooren, H. Kolstein, Fatigue assessment for deck plates in orthotropic bridge decks, *Steel Constr* 5 (2) (2012) 93–100.
- [33] C. Cui, Q. Zhang, Y. Luo, H. Hao, J. Li, Fatigue reliability evaluation of deck-to-rib welded joints in osd considering stochastic traffic load and welding residual stress, *International journal of fatigue* 111 (2018) 151–160.
- [34] Q. Zhang, Y. Ma, C. cui, X. Chai, S. Han, Experimental investigation and numerical simulation on welding residual stress of innovative double-side welded rib-to-deck joints of orthotropic steel decks, *Journal of Constructional Steel Research* 179 (2021) 106544.
- [35] W. Kong, W. Huang, Y. Wei, Numerical study on welding residual stress by double sided submerged arc welding for orthotropic steel deck, *Engineering Structures* (2024) 117445.

- [36] H. He, Q. Wang, L. Wang, B. Ji, Predicting the fatigue life of double-sided rib-to-deck welds: A single-crack propagation model and parametric investigations, *Structures* (2025) 108624.
- [37] E. Van Puymbroeck, G. Van Staen, N. Iqbal, H. De Backer, Residual weld stresses in stiffener-to-deck plate weld of an orthotropic steel deck, *Journal of Constructional Steel Research* 159 (2019) 534–547.
- [38] F. Jiang, Z. Fu, B. Ji, L. Wan, Fatigue life evaluation of deck to u-rib welds in orthotropic steel deck integrating weldment size effects on welding residual stress, *Engineering Failure Analysis* 124 (2021) 105359.
- [39] N. van den Berg, H. Xin, M. Veljkovic, Effects of residual stresses on fatigue crack propagation of an orthotropic steel bridge deck, *Materials & Design* 198 (2021) 109294.
- [40] S. Kainuma, Y.-S. Jeong, M. Yang, S. Inokuchi, Welding residual stress in roots between deck plate and u-rib in orthotropic steel decks, *Measurement* 92 (2016) 475–482.
- [41] D. Malschaert, M. Veljkovic, J. Maljaars, Numerical simulations of residual stress formation and its effect on fatigue crack propagation in a fillet welded t-joint, *Engineering Fracture Mechanics* 306 (2024) 110236.
- [42] I. Kountouris, M. Baker, Defect assessment. analysis of defects detected by mpi in an offshore structure, Tech. rep., ESLIC report no. OR6, London, U.K.: Imperial College (1989).
- [43] D. Leonetti, J. Maljaars, H. B. Snijder, Fitting fatigue test data with a novel sn curve using frequentist and bayesian inference, *Int J Fatigue* 105 (2017) 128–143.
- [44] A. Zhu, S. Ouyang, Y. Chen, Y. Sun, Fatigue test and life evaluation of rib-to-deck connections in orthotropic steel bridge decks, *Journal of Constructional Steel Research* (2022) 107442.
- [45] R. kai You, D. qing Zhang, Study on fatigue performance of u rib to deck connection with double sided welding in orthotropic steel bridge deck, *Journal of China & Foreign Highway* 38 (2018) 174–179.
- [46] W. Nagy, *Fatigue assessment of orthotropic steel decks based on fracture mechanics*, Doctoral thesis, Ghent University (2017).
- [47] H. Yuan, Optimization of rib-to-deck welds for steel orthotropic bridge decks, Tech. rep., Virginia Polytechnic Institute and State University (2011).
- [48] J. Chen, C. Wei, Y. Zhao, Fatigue resistance of orthotropic steel deck system with doubleside welded rib-to-deck joint, *Advances in Structural Engineering* 0 (2022) 1–14.

- [49] H. Yang, P. Wang, H. Qian, S. Niu, P. Dong, An experimental investigation into fatigue behaviors of single- and double-sided u rib welds in orthotropic bridge decks, *Int J Fatigue* 159 (2022) 106827.
- [50] Z. Zhu, J. Li, X. Chen, A. Carpinteri, Stress behaviors of rib-to-deck double-sided weld detail on orthotropic steel deck, *J Constr Steel Res* 187 (2021) 106947.
- [51] B. zhong Pang, C. Cui, Q. song Zheng, K. wen Liu, Q. hua Zhang, Multi-crack propagation analysis of double-side welded rib-to-deck joint in orthotropic steel decks, *Journal of Constructional Steel Research* (2024) 108731.
- [52] Q. Zhang, J. Li, D. Yuan, Y. Bu, G. Xu, Fatigue performance of rib-to-deck joint in orthotropic steel bridge deck with new type of both-side fillet welded joints, in: *Proceedings of the 40th IABSE Symposium, Nantes, France, 2018*, pp. 19–21.
- [53] S. Ya, K. Yamada, T. Ishikawa, Fatigue evaluation of rib-to-deck welded joints of orthotropic steel bridge deck, *J Bridge Eng* 16 (4) (2011) 492–499.
- [54] W. Wu, M. Veljkovic, H. Kolstein, R. Pijpers, J. Maljaars, Fatigue behaviour of root crack in stiffener-to-deck plate weld at crossbeam of orthotropic bridge decks, *Engineering Structures* 306 (2024) 117710.
- [55] C. Dung, E. Sasaki, K. Tajima, T. Suzuki, Investigations on the effect of weld penetration on fatigue strength of rib-to-deck welded joints in orthotropic steel decks, *Int J Steel Struct* 15 (2015) 299–310.